PRODUCING AND ISOLATING A ^{59}Fe BEAM USING TEXAS A&M'S MARS

by

Parker Neilson

A senior thesis submitted to the faculty of

Brigham Young University - Idaho

in partial fulfillment of the requirements for the degree of

Bachelor of Science

Department of Physics

Brigham Young University - Idaho

April 2025

BRIGHAM YOUNG UNIVERSITY - IDAHO

DEPARTMENT APPROVAL

of a senior thesis submitted by

Parker Neilson

This thesis has been reviewed by the research committee, senior thesis coordinator, and department chair and has been found to be satisfactory.

Date	Kevin Kelley, Advisor
Date	Matt Zachreson, Committee Member
Date	Todd Lines, Committee Member
Date	Department Chair, Evan Hansen

ABSTRACT

PRODUCING AND ISOLATING A ^{59}Fe BEAM USING TEXAS A&M'S MARS

Parker Neilson

Department of Physics

Bachelor of Science

We investigated the production of ^{59}Fe beams for nuclear astrophysics studies, particularly its role in stellar nucleosynthesis and ^{60}Fe production. Using sputtered ^{58}Fe, we accelerated the ions into a deuterium and Havar target, producing exotic nuclei in-flight. The Texas A&M Momentum Achromat Recoil Separator (MARS) spectrometer separated nuclides by magnetic rigidity, while LISE++ (the software model of MARS) predicted energy losses in a ΔE–E_{res} silicon detector. We successfully isolated ^{59}Fe from nuclides of mass 58. However, ^{59}Co, sharing the same mass, was inseparable by mass selection alone. Its extra proton allowed partial differentiation using statistical analysis of ΔE vs. position and E_{res} vs. position graphs.

ACKNOWLEDGMENTS

Thanks to the Department of Energy (DE-FG02-93ER40773) and the National Science Foundation (PHY-2051072) for helping me get this research opportunity for me. I'm also grateful to Texas A&M's Cyclotron Institute, in particular Dr. Roeder, for helping me explore the field of nuclear physics.

Contents

List of Figures

Chapter 1

Introduction

Stellar chronometry, the study of the age of stars and the dating of stellar-related events, relies heavily on the characteristic γ rays emitted by decaying isotopes. Among these, the decays of ^{60}Fe and ^{26}Al stand out as especially important. The flux ratio of these two isotopes (that is, the ratio ^{60}Fe/^{26}Al) has been shown not to match stellar models [1, 2]. It has also been shown in previous studies that the stellar decay rate of ^{59}Fe has significant implications for ^{60}Fe radioactivity in massive stars [1]. The decay rate of ^{59}Fe has been measured thoroughly, but its decay rate in stellar environments has enough uncertainty to warrant a deeper investigation [2]. The half-life of ^{59}Fe is about 44 days [3], so it is rare to find outside of a stellar environment. This poses the challenge of making and studying ^{60}Fe in an environment as close to a star's as possible.

Researchers at Texas A&M's Cyclotron Institute have been trying to do just that. By using an "in-flight" technique, a beam of heavy ions can be used to make a beam of exotic ions. This works by ionizing and then accelerating a naturally occurring isotope to energies near those found in a stellar environment into a deuterium target, which allows for neutron capture. Then, while the ions are still in flight, the Momentum

Achromat Recoil Separator (MARS), a mass spectrometer, splits the beam into many beams based on mass. This allows for a pure beam of ions with a given magnetic rigidity (also called Bρ, see section 2.2) to be studied independently from all else and prevents problems stemming from doing more traditional forward kinematics, whereby light ions are accelerated into a dense target. In-flight techniques allow ions to be studied at the energies they were created at, which is why it was the chosen method.

In forward kinematics, when neutron capture happens it is often chemically identical to the target, making it difficult to isolate. Inverse kinematics, also called the "in-flight" technique, avoids this problem in exchange for another. MARS can separate beams of a given energy by their magnetic rigidity, but if there is an isobar (a nuclide of the same mass but distinct Z-number) in the beam of interest, it is effectively impossible for MARS to separate them.

To produce a beam of ^{59}Fe, atoms from a ^{58}Fe source are sputtered, ionized, and then fed into the cyclotron. There, the ions are accelerated and fed into MARS, where some of the ^{58}Fe nuclei become ^{59}Fe through neutron capture. The chamber containing deuterium is sealed by a film of Havar, an alloy made primarily of ^{59}Co; this film acts as a second target for the beam, and because of it, ions of ^{59}Co join the beam. As the beam continues through MARS, the ions of ^{59}Fe and those of ^{59}Co stay together. Together, they make one distinct mass-59 beam that collides with a detector at the end of the beamline.

From there, the process of beam identification begins. With some educated guesswork, the primary ^{58}Fe beam at charge state +23 could be assumed. From there, MARS physically blocked the ^{58}Fe beam, and data could be taken on the much less intense mass-59 beam. A range of Bρ values was measured, as Bρ does change the cross-section of ^{59}Fe.

While not separable by MARS spatially, these two isobars could be distinguished by how they interact with the detector. Atoms with a higher Z-number experience more stopping power in a given substrate than atoms of the same mass with fewer protons. In this way, we could statistically distinguish two distributions of energies deposited into the silicon detector—one for each isobar. From there, statistical methods could be used to approximately count the number of each isobar. These counts could then be normalized, and production rates and their uncertainties could be calculated. From this, the production rates of ^{59}Fe and ^{59}Co could be compared against Bρ in the hope of minimizing ^{59}Co and maximizing ^{59}Fe with respect to one another.

In this thesis, background information about the various tools, software, and instruments will be covered, followed by a detailed description of how the data was collected and analyzed. Following that will be the results and their analysis. Finally, there will be a conclusion and summary at the end.

Chapter 2

Background

This chapter provides an overview of the experimental setup and analysis tools used in this study. The primary focus is on the Momentum Achromat Recoil Separator (MARS) and its role in ion separation, as well as the key principles underlying the identification and characterization of isotopes. Additionally, the computational tools employed for data analysis, including CERN's ROOT and LISE++, are introduced.

2.1 MARS

MARS functions as a mass spectrometer with a built-in target for the primary beam. It operates by separating ions using a series of dipole and quadrupole magnets, as well as physical slits. A single beam enters MARS, and as it passes through the dipole magnets, it is split into multiple beams of distinct magnetic rigidity (Bρ, see Section 2.3).

A dewar cooling an airtight chamber is filled with liquid nitrogen. Deuterium is then introduced into the chamber. The drop in temperature increases the density of deuterium, resulting in more collisions and thus a greater production of ^{59}Fe. The

chamber is sealed with a film of Havar, a cobalt-based alloy. Havar is used due to its increased ductility under cryogenic conditions [4]. Its ability to withstand high pressures at low temperatures makes it one of the rare materials capable of sealing the chamber under atmospheric pressure at both room and liquid nitrogen temperatures. Consequently, the beam effectively encounters two targets: Havar as it enters and exits the chamber, and deuterium as it moves within the chamber. Notably, ^{59}Co is the most common isotope of cobalt and has the same mass as ^{59}Fe, making it difficult to isolate. This posed a significant challenge in the separation of ^{59}Fe.

After interacting with the targets, the beam passes through additional dipole magnets to separate the newly added mass-59 ions from the primary mass-58 beam. Slits, which function like sliding doors, are used as needed to physically block unwanted portions of the beam. Multiple slits are distributed throughout MARS. Quadrupole magnets are also used to focus the beam as necessary. Figure 2.1 below illustrates the beam path, which enters on the right and moves to the left.

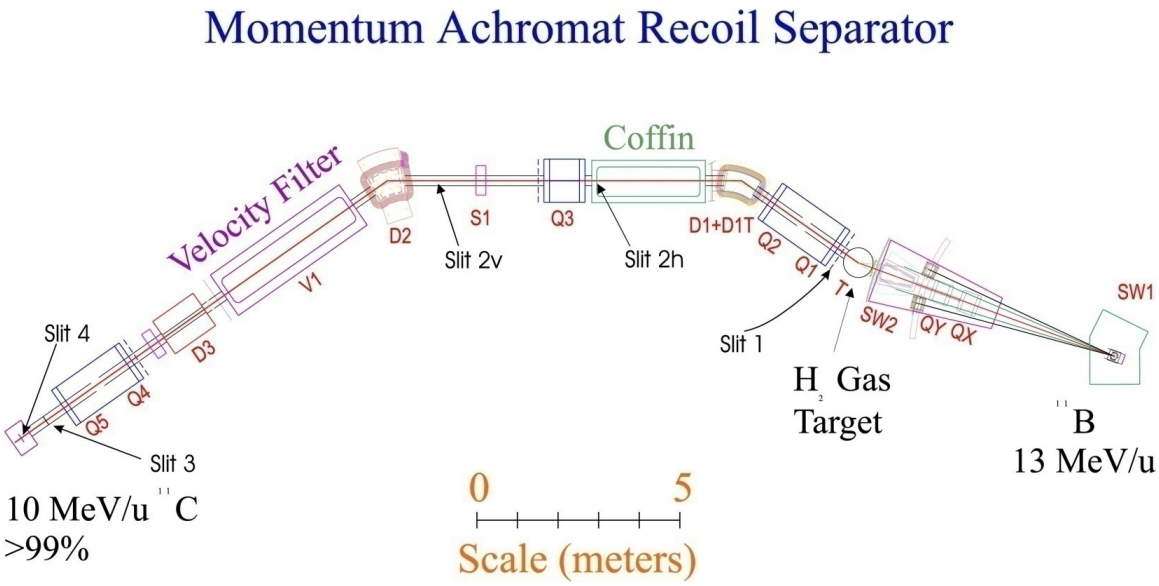

Figure 2.1 MARS diagram, adapted from [5]

2.2 Magnetic Rigidity (Bρ)

Bρ is defined in equation 2.1 where $\vec{B}$ represents the magnetic field, and $\vec{\rho}$ is the radius of curvature for a charged particle with momentum perpendicular to the field, q is the charge state, and $\vec{p_\perp}$ is the momentum, which is mutually perpendicular to both $\vec{\rho}$ and $\vec{B}$.

$$|\vec{B}| \cdot |\vec{\rho}| = \frac{|\vec{p_\perp}|}{q} \tag{2.1}$$

Bρ is a scalar value typically expressed in Tesla meters. Bρ is used because it captures both the charge-to-mass ratio as well as the momentum of the particle. This is all of the information needed to find the trajectory of a charged particle through a known electromagnetic field.

2.3 Silicon Detector

The detector consists of two components: the outer ΔE detector and the inner residual energy (E$_{res}$) detector. The ΔE detector absorbs some, but not all, of the energy of incident ions while also measuring the impact location. The E$_{res}$ detector is a simple silicon slab that measures the remaining energy of the ion. The total energy of a particle, E$_{tot}$, is the sum of ΔE and E$_{res}$:

2.4 CERN's ROOT

Much of the data visualization for this experiment was performed in ROOT, and several figures used in this study were generated using this software. Detectors for particle collisions often generate immense amounts of data, often in the terabyte range.

Storing such data in a tabular format and loading it into RAM is impractical. Instead, traditional file types and analysis methods are replaced with binary tree (.root) files, which are analyzed using the open-source data analysis framework ROOT. Originally developed at CERN, ROOT has since been adopted for various data analysis applications. Its object-oriented C++ structure makes it highly adaptable but also introduces complexity. For this reason, the data was automatically stored in a .root file, requiring those working on the project to work with the software [6].

2.5 LISE++

LISE++, referred to here as LISE, is a model version of MARS. The primary functionality of LISE relevant to this project is its physical calculator. By inputting the Bρ, atomic number (Z), mass number (A), and charge state of a given beam, LISE returns the expected ΔE and E_{res} values that the detector should record [7].

Chapter 3

Methods

This chapter details the procedures used to identify, isolate, and analyze the relevant ion beams in the experiment. The methodology is structured to first establish the presence of the desired isotopes, then refine their separation, and finally calibrate and quantify the production rates. Each step is crucial to ensure accurate and reliable results, leveraging experimental techniques such as magnetic rigidity tuning, energy loss differentiation, and beam normalization.

3.1 Creation and Separation of the Mass 58 and 59 Beams

To make the beam, ^{58}Fe atoms are separated from the source (a nearly pure sample of ^{58}Fe) in a process called sputtering. These are then ionized to a number of charge states, generally in the range of +22 to +24 in an Electron Cyclotron Resonance machine. Once ionized, the ^{58}Fe is fed into the cyclotron and accelerated. Once sufficiently accelerated, the ions are directed into MARS.

When the beam is activated, the specific ions striking the detector at the end of

MARS are initially unknown. Thus, the ion identification process begins.

The process of beam separation begins in the "coffin" (see Figure 2.1, labeled in green). Figure 3.1 is a picture of the coffin. Remote monitoring of the coffin allows a controller in a safe location to navigate beams through a hole in the coffin's rear via the electromagnets. Those in the control room had power to adjust the beam attenuation, slit positions, and the current in the magnets.

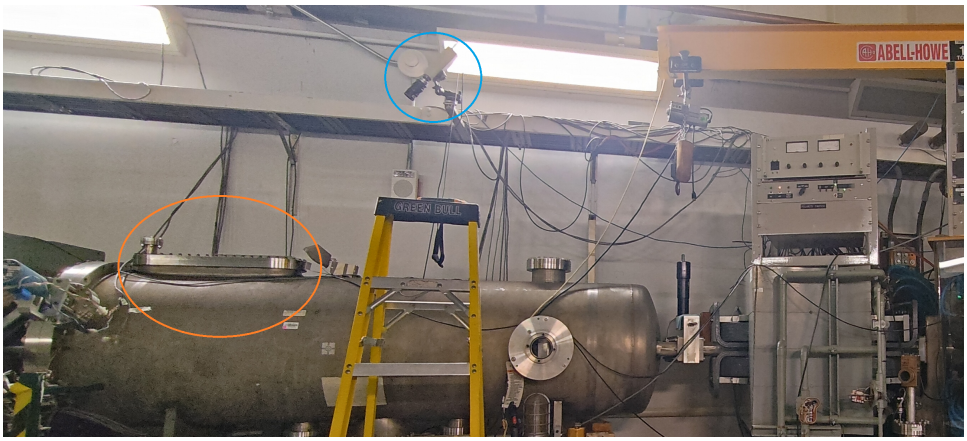

Figure 3.1 The Coffin is the large metal tank occupying the bottom left portion of this image. The blue circle is a CCTV camera that allows for remote monitoring of the beam's path through the opening circled in orange.

The mass 59 beams were separated from mass 58 by adjusting remotely controlled slits. Once the primary beam was sufficiently blocked, attenuation was removed, and data collection proceeded for several minutes. This procedure was conducted across a number of charge states, but analysis was only conducted on the +23 state, as this state has the greatest beam intensity.

3.2 Calibration

At this stage, the suspected ^{59}Fe beam required further verification. Confirmation was only possible through LISE analysis. Each charge state exhibits a range of Bρ

values that allow it to interact with the detector. Each of these Bρ values has been shown to change the nuclear cross-section of ^{58}Fe and thus also the production rate of ^{59}Fe. Previous work established a relationship between the magnetic field and magnet current, stored in an Excel spreadsheet. By inputting the current, the spreadsheet calculates the Bρ in Tm. LISE needs Bρ to determine how the beam will interact with the detector.

Using ROOT and custom macros, an uncalibrated distribution of the mass 59 beam was generated, revealing two distinct but overlapping distributions, as shown in Figure 3.2.

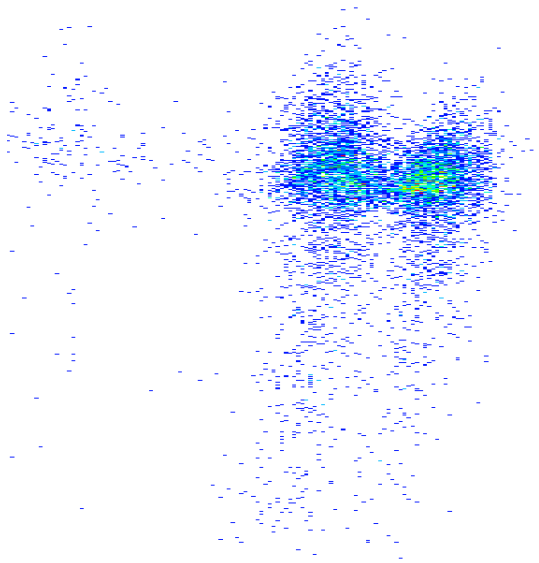

Figure 3.2 Overlapping distributions of what is suspected to be ^{59}Fe and ^{59}Co plotted on an uncalibrated ΔE vs E$_{res}$ plot in ROOT's TBrowser.

MARS is limited in its ability to separate ions with similar Bρ values. Since Bρ is defined as $\frac{|\vec{p_\perp}|}{q}$, ions with similar momentum and the same charge state will remain nearly indistinguishable. The mass difference between ^{59}Co (58.93319 amu) and ^{59}Fe (58.934873 amu) is small, preventing further separation using MARS alone [8]. Differentiation was instead achieved using stopping power, described by Equation 3.1.

$$-\frac{dE}{dx} \propto \frac{Z^2}{A} \cdot \frac{Z_{\text{target}}}{\beta^2} \tag{3.1}$$

Since Z_{target}, A, and β are nearly identical for both beams, energy deposition differs due to the Z^2 dependency. This distinction was leveraged using the ΔE and E_{res} detectors, which naturally differentiated the ions.

Calibration was performed by mapping default detector settings to LISE predictions. The LISE physical calculator provided expected energy depositions, which were used to align the center of each distribution. Post-calibration, the ^{59}Co distribution aligned precisely with LISE predictions, confirming the calibration process. Below are the LISE++ predictions for one of the Bρ values measured.

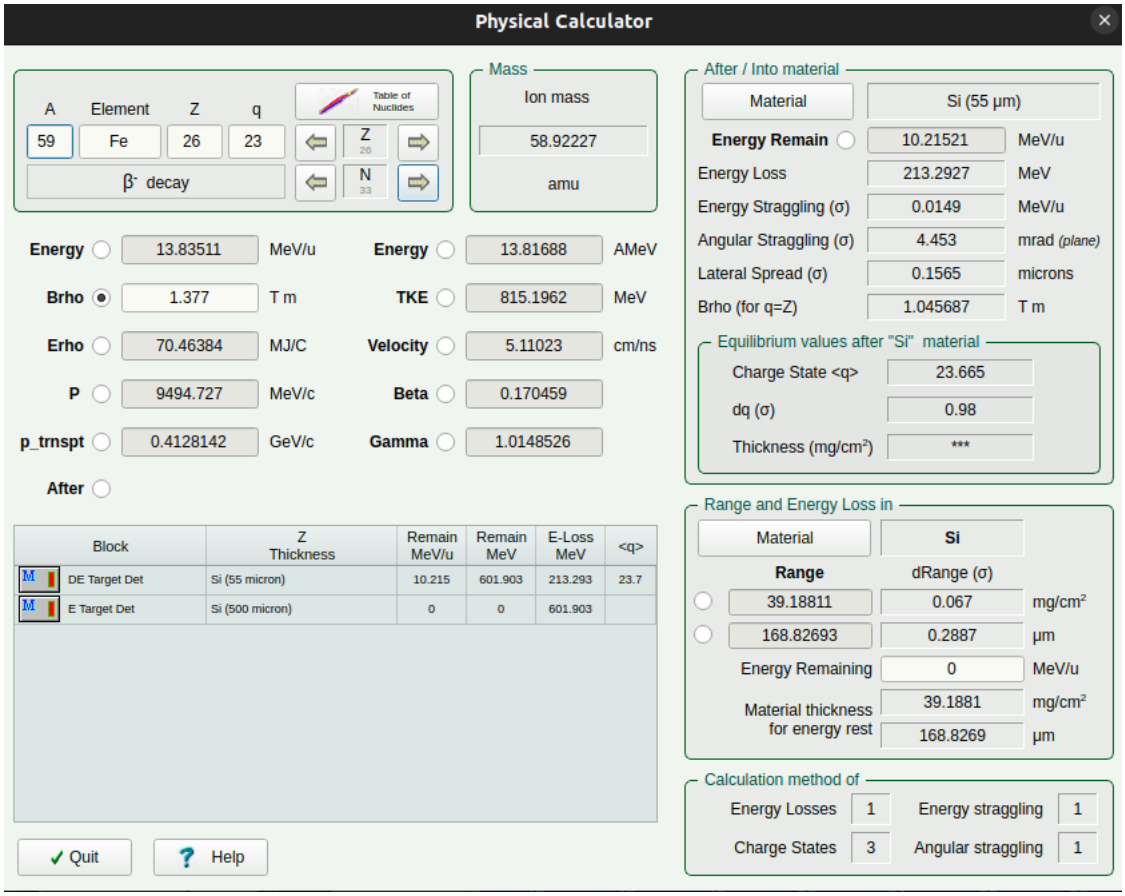

Figure 3.3 LISE++ physical calculator. The box in the top left allows users to characterize the beam's composition. Beneath that box, Bρ is input. The outputs are given for each part of the detector DE (ΔE) and E (E_{res}) in the bottom left box. These outputs are the modeled energy losses experienced by incident ions on each of the detectors.

3.3 Calculation of Production Rates

To determine production rates, relevant data was isolated by applying selection gates, as illustrated in Figure 3.4.

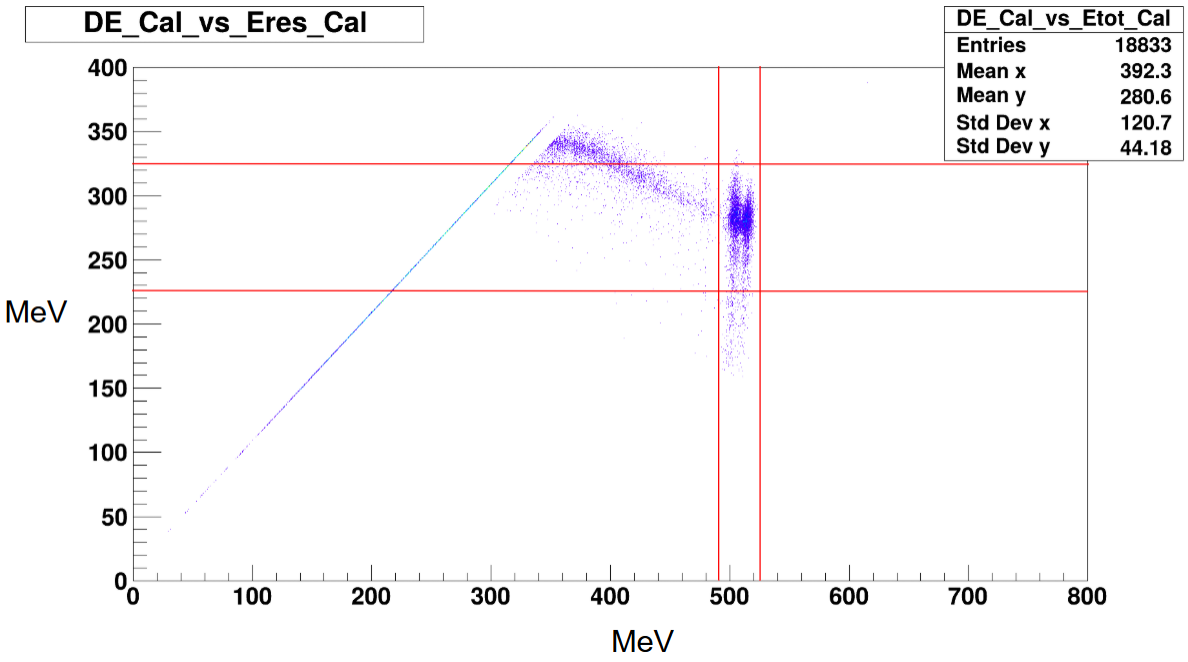

Figure 3.4 Gated Data: 2D distribution of ΔE vs E_{res} displayed in ROOT. The area enclosed by the red lines is demonstrative of the gated dataset. Note that ΔE is along the x-axis.

The gated data was exported from ROOT to a .csv file. Peaks in the projected ΔE distribution were identified found manually using visual estimation. The assumption of symmetric peaks facilitated distinguishing ^{59}Co from ^{59}Fe. Figure 3.5 is not taken from real data, but it demonstrates how the peaks appear when projected onto the ΔE axis. Taking the area shaded in blue to be entirely composed of counts from ^{59}Co and doubling it gives the total number of ^{59}Co ions that collided with the detector. The rest of the counts were taken to be ^{59}Fe.

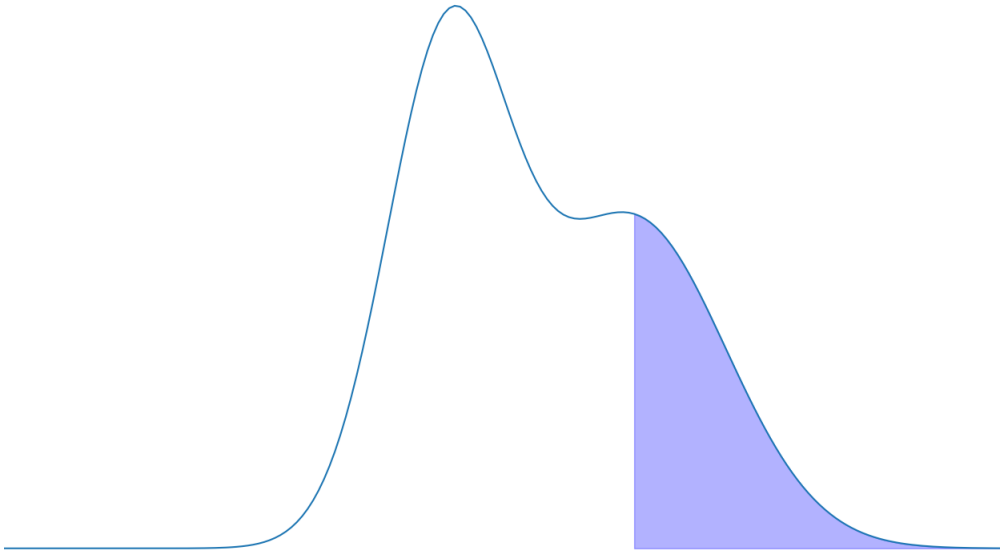

Figure 3.5 Overlapping distributions of ^{59}Co on the right and ^{59}Fe on the left. The shaded region is assumed to be entirely composed of ^{59}Co collision readings.

Normalization of the counts (C) was performed using beam current measurements, recorded on a 0.6 nA scale at a 1 kHz pulse frequency. The number of pulses was recorded for each run. The normalization factor M was determined as follows:

$$0.6 \text{ nA} = 0.6 \text{ nC} \cdot \text{s}^{-1} \tag{3.2}$$

$$\frac{0.6 \text{ nC} \cdot \text{s}^{-1}}{1000 \text{ pulses} \cdot \text{s}^{-1}} = 0.0006 \text{ nC} \cdot \text{pulse}^{-1} \tag{3.3}$$

$$0.0006 \text{ nC} \cdot \text{pulse}^{-1} \cdot N \text{ pulses} = M \text{ nC} \tag{3.4}$$

The normalized counts were then calculated using Equation 3.5:

$$\text{Normalized Counts} = \frac{C}{M} \text{ counts/nC} \tag{3.5}$$

Finally, uncertainties in both counts and normalization were determined. This provided the production rate in counts/nC for each Bρ value.

Chapter 4

Results

This chapter presents the results of the production rate measurements as a function of the magnetic rigidity ($B\rho$) for charge state +23. The data is displayed graphically, highlighting key trends and uncertainties. Following this, an analysis is provided to interpret the relationship between $B\rho$ and the production rates of ^{59}Fe and ^{59}Co, with a focus on optimizing the beam purity for experimental applications.

4.1 Display of Results

Below is the plot of production rate vs Bρ with their uncertainties for charge state +23.

The production rate of ^{59}Fe was measured at its highest when Bρ is 1.092 Tm. This coincides with the lowest production rate of ^{59}Co at the same Bρ. It is important to recall that what we measure is effectively the cross section of ^{58} Fe. What is wanted is to increase the cross-section of ^{59}Fe while minimizing the ^{59}Co, so that we have a beam of pure ^{59}Fe. The range of Bρ values tested contain a distinct peak in the production rate of ^{59}Fe.

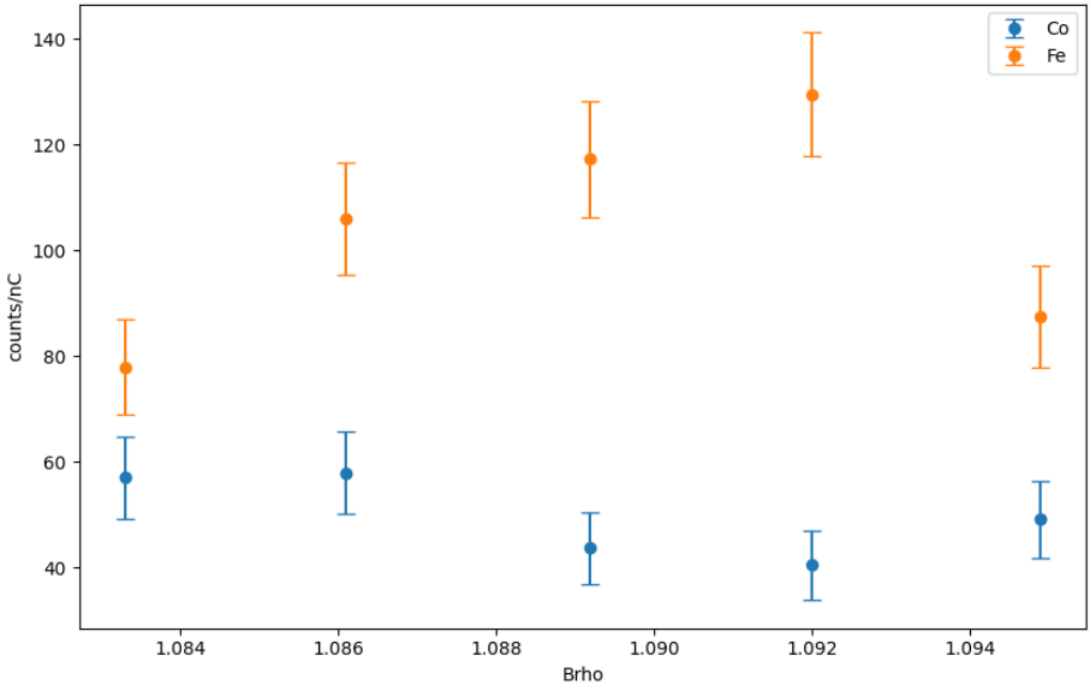

Figure 4.1 Production Rate vs Bρ

4.2 Analysis of Results

Given the current configuration of MARS with its havar coverings, the Bρ at 1.092 Tm is the ideal place to run the beam through to maximize the production rate of Fe, and minimize Co.

Chapter 5

Conclusion

This thesis has explored the production and isolation of ^{59}Fe beams, with a particular focus on the charge state +23. These efforts gave a deeper understanding of how Bρ relates to the cross-section of both ^{59}Fe and ^{59}Co. The results indicated that the Bρ around 1.092 Tm yielded both the highest production of ^{59}Fe and the lowest of ^{59}Co. These results could, someday, give us a deeper understanding of the nature of ^{60}Fe.

A more efficient and controlled production of ^{59}Fe enables more precise studies of its decay pathways and behavior in conditions mimicking stellar interiors. Since ^{59}Fe is a key progenitor of ^{60}Fe—a radioactive isotope whose γ-ray signatures help astronomers trace stellar life cycles. By refining how we isolate and study these short-lived isotopes on Earth, we take one step closer to resolving the discrepancies between stellar models and observational data, ultimately deepening our grasp of the life and death of stars.

Bibliography

[1] B. Gao, S. Giraud, K. A. Li, X. Xu, H. L. Wang, Y. B. Wang, et al., "New ^{59}Fe Stellar Decay Rate with Implications for the ^{60}Fe Radioactivity in Massive Stars," *Physical Review Letters*, **126**, 152701 (2021). https://doi.org/10.1103/PhysRevLett.126.152701.

[2] EurekAlert, "Study Sheds Light on Radioactive Isotopes in Massive Stars," *EurekAlert News Release*, (2021). Available at: https://www.eurekalert.org/news-releases/740712.

[3] A. Yunoki, Y. Sato, L. Joseph, A. Ravindra, D. B. Kulkarni, M.-C. Yuan, K. B. Lee, J. M. Lee, A. Agusbudman, T.-S. Park, P. A. L. da Cruz, C. J. da Silva, A. Iwahara, M. Zhang, J. C. Liang, H. R. Liu, M. J. van Staden, J. Lubbe, M. W. van Rooy, B. R. S. Simpson, P. Paukkachane, N. Sastri, T. Soodprasert, P. Marsoem, H. C. Holnisar, and G. Wurdiyanto, "Report of APMP Comparison of the Activity Measurements of ^{59}Fe (APMP.RI(II)-K2.Fe-59)," *Bureau International des Poids et Mesures (BIPM)*, (2017). Available at: https://www.bipm.org/documents/20126/48150627/APMP.RI

[4] H. F. Hobart and C. J. Morris, "Evaluation of Havar Foil for Cryogenic Applications," *Los Alamos Scientific Laboratory Report*, **LA-6345** (1976). https://www.osti.gov/servlets/purl/7230523.

[5] B. Roeder, "Methods of Radioactive Beam Production," *Cyclotron Institute, Texas A&M University*, 19 June 2017.

[6] CERN. (2024). *ROOT: Data Analysis Framework*. Retrieved March 28, 2024, from https://root.cern/about/

[7] MSU FRIB. (2024). *LISE++: Exotic Beam Production and Simulation*. Retrieved March 28, 2024, from https://lise.frib.msu.edu/lise.html

[8] Isotope Browser. (n.d.). Cobalt-59 and Iron-59 Atomic Mass. Retrieved March 29, 2024, from https://play.google.com/store/apps/details?id=iaea.nds.nuclides&hl=en_US&pli=1